Journal of Organometallic Chemistry, 479 (1994) 59–72

Synthesis and structural characterization of the isomers of $Rh_6(CO)_{14}L_2$ clusters (L = NCMe, Py, $P(OPh)_3$), X-ray crystal structure of *trans*-$Rh_6(CO)_{14}\{P(OPh_3)\}_2$

S.P. Tunik, A.V. Vlasov, K.V. Kogdov, G.L. Starova and A.B. Nikol'skii

St. Petersburg University, Department of Chemistry, Universitetskii pr., 2, 198904 St. Petersburg (Russian Federation)

O.S. Manole and Yu.T. Struchkov

A.N. Nesmeyanov Institute of Organoelement Compounds, 28 Vavilov Street, 117813 Moscow (Russian Federation)

(Received September 21, 1993)

Abstract

The reaction of $Rh_6(CO)_{16}$ with two equivalents of Me_3NO in the presence of a substituting ligand (L = NCMe, Py, $P(OPh)_3$) affords a mixture of isomers of the general formula $Rh_6(CO)_{14}L_2$. The substituting ligands occupy two terminal sites in the structure of the parent cluster. For L = $P(OPh)_3$ three isomers (I–III) were separated from the reaction mixture. The structure of the first isomer (I) has been established by X-ray analysis. This compound crystallizes in two polymorphic modifications, monoclinic and triclinic; both of which consist of identical molecules and differ only in the packing of the molecules in the crystals. It should be noted that both polymorphic forms contain in the unit cells the racemic mixture (RR and SS) of the $Rh_6(CO)_{14}\{P(OPh)_3\}_2$ molecules. This octahedral cluster may be considered as a derivative of the parent $Rh_6(CO)_{16}$ cluster with two terminal CO groups in *trans* positions at Rh(1) and Rh(2) atoms substituted by phosphite ligands. The structures of two other disubstituted clusters, (II) and (III) were established by ^{31}P NMR spectroscopy. Phosphite ligands in these compounds occupy the terminal sites at the adjacent rhodium atoms of the Rh_6 octahedron but differ in their mutual orientation. Other disubstituted derivatives (L = NCMe, Py) are labile compounds and exist in solution as inseparable mixtures of the isomers characterized by ^1H and ^{13}C NMR spectroscopy. A mechanism of interconversion of the isomers is proposed.

Key words: Rhodium; X-ray diffraction; Carbonyl; Cluster; Nuclear magnetic resonance; Isomerism

1. Introduction

The reactivity of coordination compounds depends to a great extent on the mutual disposition and mutual influence of ligands. The mechanisms of such influence are sufficiently well understood for mononuclear complexes, but for cluster compounds the same problems are considerably complicated by the polynuclearity of the metal core. Successive substitution of several carbonyl ligands in homoleptic carbonyl clusters gives rise to the problem of preferential sites for the second and further substitutions, *i.e.* to the problem of the influence of the heteroligand upon reactivity of different coordination positions. The number of possible sites for substitution in the case of clusters is much greater than with mononuclear compounds, and mechanisms for the mutual influence of ligands have not yet been studied in detail, especially for clusters with nuclearity greater than four. This problem was first studied for $Os_6(CO)_{16}L_2$ complexes with bicapped tetrahedral metal core and for $Os_6(CO)_{21-x}\{P(OMe)_3\}_x$ ($x = 1$–6) clusters with the planar raft Os_6 framework [1]. In the latter case all possible isomers were obtained using different synthetic methods and characterized with X-ray analysis and ^{13}C, ^{31}P NMR. Following this line in

Correspondence to: Dr. S.P. Tunik.

0022-328X/94/$7.00
SSDI 0022-328X(93)24308-R

the present paper we carried out the synthesis and structural characterization of the disubstituted derivatives $Rh_6(CO)_{14}L_2$ of the octahedral rhodium cluster obtained by the reaction of $Rh_6(CO)_{16}$ with the corresponding ligands (L = NCMe, Py, $P(OPh)_3$) promoted by Me_3NO.

2. Results and discussion

2.1. General discussion

In previous papers [2–4] we studied CO substitution reactions in $Rh_6(CO)_{16}$. A series of the monosubstituted derivatives $Rh_6(CO)_{15}L$ with various N- and P-donor ligands has been prepared and structurally characterized. Disubstituted derivatives of $Rh_6(CO)_{16}$ can easily be synthesized by the following reaction

$$Rh_6(CO)_{16} + L \xrightarrow[CHCl_3]{+2\ Me_3NO} Rh_6(CO)_{14}L_2 \qquad (1)$$

L = NCMe, Py, $P(OPh)_3$

In all cases initial chromatographic separation of the reaction mixture gives, as a main band, a compound with the stoichiometry of the disubstituted cluster $Rh_6(CO)_{14}L_2$. However, the NMR spectral characteristics of the products obtained are too intricate to belong to individual compounds and indicate the presence of isomers of $Rh_6(CO)_{14}L_2$ in the separated bands. As shown earlier [2–4], two electron ligands substitute terminal CO groups only in the structure of the parent $Rh_6(\mu_3\text{-}CO)_4(CO)_{12}$ cluster. This suggests the existence of five possible isomers with the different mutual disposition of two heteroligands in the twelve terminal sites. These isomers are schematically shown in Fig. 1, and at least several of them are formed in the course of reaction (1). It should be noted that the behaviours of the isomers obtained differ significantly for each kind of ligand used and these are discussed separately below.

2.2. L = P(OPh)$_3$

Careful chromatographic separation of the $Rh_6(CO)_{14}\{P(OPh)_3\}_2$ mixture gives two bands, one of which contains individual compound (I) which was characterized by a single crystal X-ray analysis and ^{13}C, ^{31}P NMR spectroscopy. The other band contains an inseparable mixture of two isomers (compounds (II) and (III)), their structure having been determined by simulation of the ^{31}P NMR spectrum of the mixture.

An X-ray structure study has shown that monoclinic (IA) and triclinic (IB) crystal modifications (IA) contain molecules with very similar structures (Figs. 2–4). All these molecules have an idealized C_2 symmetry (the symmetry axis coincides with the Rh(3)–Rh(5) direction), *i.e.*, they are chiral. Moreover, two geometric isomers (diastereomers) of (I) are, in principle, possible. In the first isomer the CO and $P(OPh)_3$ ligands at Rh(1) and Rh(2) are directed over the "free" faces of the Rh_6 octahedron (Rh(1)Rh(3)Rh(6) and Rh(1)Rh(4)Rh(5) at Rh(1), Rh(2)Rh(3)Rh(4) and Rh(2)Rh(5)Rh(6) at Rh(2), see Fig. 2). This isomer is sterically more favourable and, indeed, is realized in the crystals of both modifications. In the second isomer

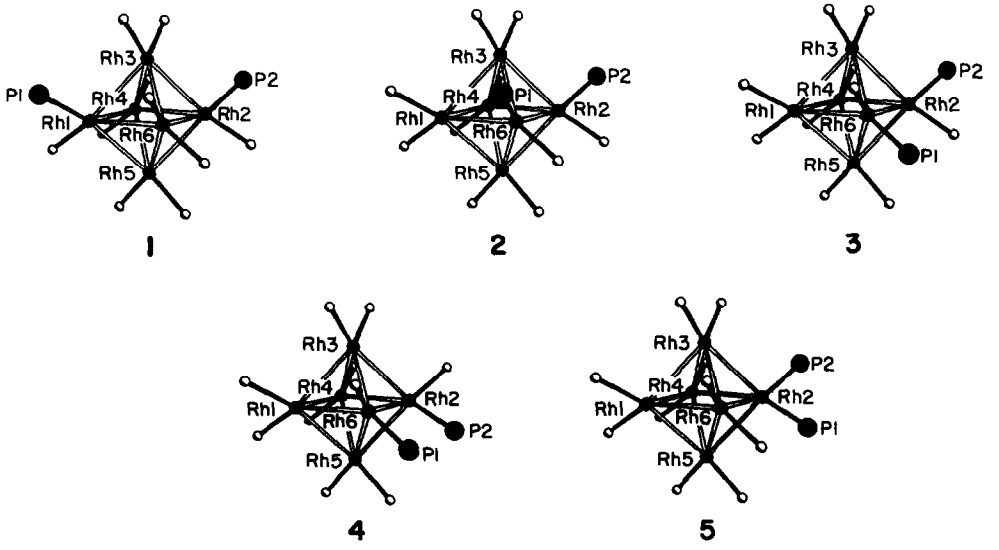

Fig. 1. Schematic representation of the five stereochemically possible isomers of $Rh_6(CO)_{14}\{P(OPh)_3\}_2$. Only rhodium and phosphorus atoms and directions of terminal Rh–CO bonds are shown.

the ligands at Rh(1) and Rh(2) are directed towards the octahedron faces with μ_3-CO-bridges (Rh(1)Rh(3)-Rh(4) and Rh(1)Rh(5)Rh(6) at Rh(1), Rh(2)Rh(4)Rh(5) and Rh(2)Rh(3)Rh(6) at Rh(2)). This isomer, however, would have been much more sterically overcrowded and, therefore, is not observed in the crystals.

The centrosymmetric crystal (IA) represents a racemate composed of IA(RR) and IA(SS) molecules (naturally, the R and S designation are arbitrary and are used by analogy with the traditional nomenclature for chiral centres; diastereomers which are not observed should be named RS and SR). Likewise the centrosymmetric crystal (IB) with two crystallographically independent molecules (a and b) may be called a "double" racemate of equal numbers of IBa(RR), IBa(SS), IBb(RR), and IBb(SS) molecules.

In the molecule (I) two phosphite ligands substitute terminal CO groups at Rh(1) and Rh(2) atoms occupying *trans*-positions in the Rh_6 octahedron. Four of the remaining CO ligands are μ_3-bridging as in the structure of $Rh_6(CO)_{16}$. General features of the molecular structures of (IA), (IBa), and (IBb) are very close to each other (see Tables 1 and 2), the molecules displaying similar systematic distortions of the Rh_6 octahedron. The Rh(3)Rh(4)Rh(5)Rh(6) plane, that does not comprise the Rh atoms bound to the phosphite ligands, contains the shortest Rh–Rh bonds (averages 2.746 (IA), 2.745 (IBa) and 2.748 Å (IBb)), whereas the four longest Rh–Rh bonds are located in positions *cis*- to $P(OPh)_3$ ligands (average 2.797 (IA), 2.794 (IBa) and 2.800 Å (IBb)). The corresponding *trans* Rh–Rh bonds average as follows 2.770 (IA), 2.772 (IBa) and 2.768 Å (IBb). The elongation of Rh–Rh bonds in positions *cis*- to PPh_3 and $P(OPh)_3$ ligands was observed earlier in other substituted $Rh_6(CO)_{16}$ derivatives [5,6]. The Rh(1)–P(1) and Rh(2)–P(2) bond lengths (av. 2.248 (IA), 2.258 (IBa) and 2.254 Å (IBb)) are comparable with the other similar distances, *e.g.*, in $Rh_4(CO)_8\{P(OPh)_3\}_4$ (av. 2.23 Å) [7] and in $Rh_6(CO)_{12}\{P(OPh)_3\}_4$ (av. 2.27 Å) [5]. The phosphite ligands in (I) show average P–O and O–Ph distances (1.593 (IA), 1.598 (IBa), 1.599 (IBb) and 1.41 (IA), 1.42 (IBa), 1.41 Å (IBb)) which are comparable with earlier data [2,4]. The local molecular C_2 symmetry of (I) is violated by phenyl rings of the triphenylphosphite ligands.

The ^{13}C and ^{31}P spectra of (I) are given in Fig. 5. The ^{31}P spectrum displays a doublet signal ($^1J(Rh-P) = 241$ Hz) which reveals, on treatment with a line

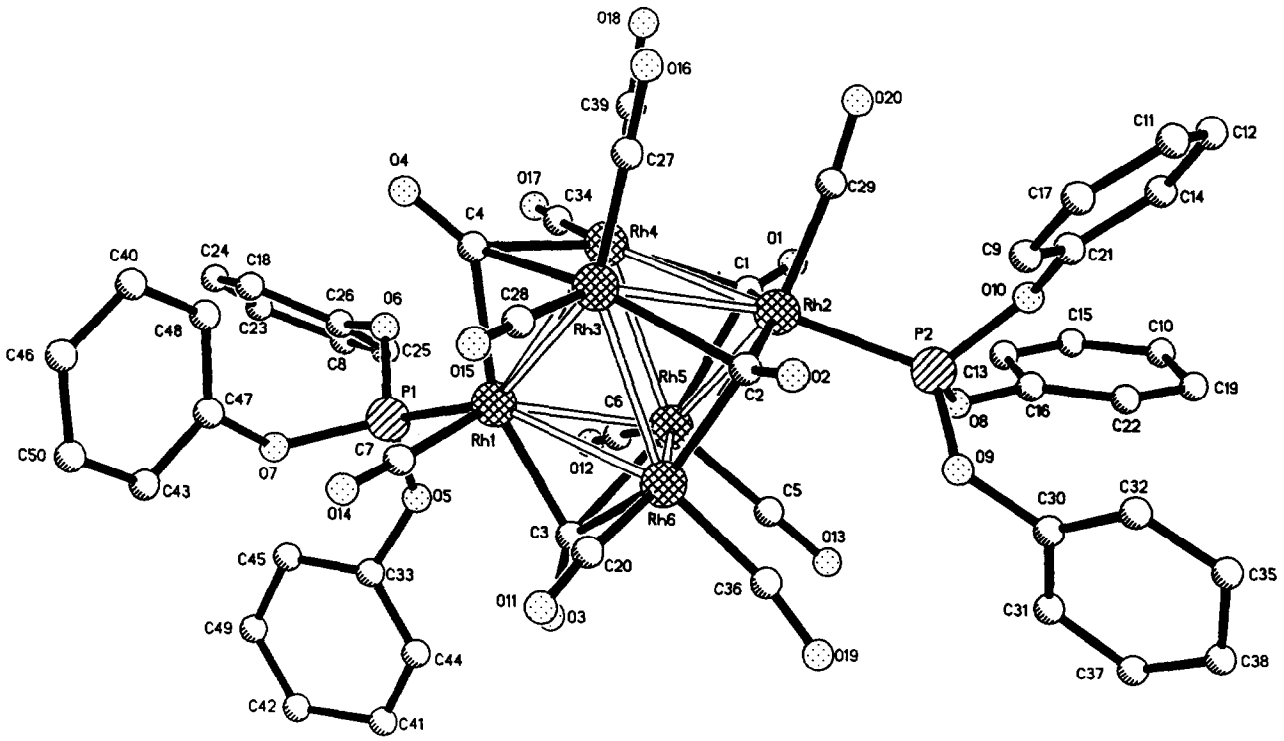

Fig. 2. Molecule IA in crystal (hydrogen atoms are omitted).

narrowing procedure, a triplet structure of the doublet components (^2J(Rh–P) = 8 Hz). The second order coupling is due to the interaction of the phosphorus atoms with only two of the four equatorial Rh atoms whose Rh–Rh bonds are in the *trans*-position to the given phosphorus atom (*e.g.*, Rh(3), Rh(6) relative to P(1) and Rh(3), Rh(4) relative to P(2)). This observation is in line with the theoretical study of $^2J_{XMY}$ couplings and a great body of experimental data [8,9].

The idealized ^{13}C spectrum of (I) in the carbonyl region should consist of two μ_3-CO quartets, four doublets of terminal CO and one doublet of doublets corresponding to terminal CO groups adjacent to phosphite ligands, each of the signals being of double intensity. In fact, the experimental spectrum (Fig. 5) displays two quartets of μ_3-CO and the dd signal of C(7)O(14) and C(29)O(20) carbonyl groups adjacent to phosphite ligands. As for the remaining terminal CO, the spectrum obtained reveals a pattern corresponding to a lower symmetry than that of the idealized C_2 molecular structure of (I). Instead of four doublets of double intensity one can observe four doublets of single intensity and one doublet of relative intensity four. Such disagreement between the experimental and idealized spectra is due to the distortions in the C_2 structure of (I) which in turn are caused by short nonbonding contacts between terminal CO groups and OPh moieties of phosphite ligands. For example, in the molecule (IA) such contacts (C(20)–C(7) 3.008, O(11)–O(14) 3.141, C(36)–O(9) 2.903, C(6)–O(5) 3.047, O(12)–O(5) 2.977 C(5)–O(8) 3.047 and O(13)–O(8) 2.985 Å) even give rise to Rh–C–O moiety bending: Rh(6)C(20)O(11) 171.0° and Rh(6)C(36)O(19) 169.6°. Similar distortions are observed in (IBa) and (IBb) as well. It should be noted that the analogous relation between ^{13}C NMR spectral parameters and nonbonding contacts of CO groups has already been pointed out [4] for the $Rh_6(CO)_{15}PPh_3$ cluster.

We failed to isolate individual compounds in the second chromatographic band even after the careful separation, and to grow single crystals suitable for an X-ray structural study. However, the ^{31}P COSY spectrum of this band (Fig. 6) clearly displays two groups of signals (excluding the admixture of (I) which is marked with an asterisk) that correspond to two individual compounds, (II) and (III). Elemental analysis of the mixture fits well the stoichiometry of the disubstituted cluster $Rh_6(CO)_{14}\{P(OPh)_3\}_2$, and we attempted to simulate its spectrum using the isomers (**2–5**) (Fig. 1) as structural and spin coupling models.

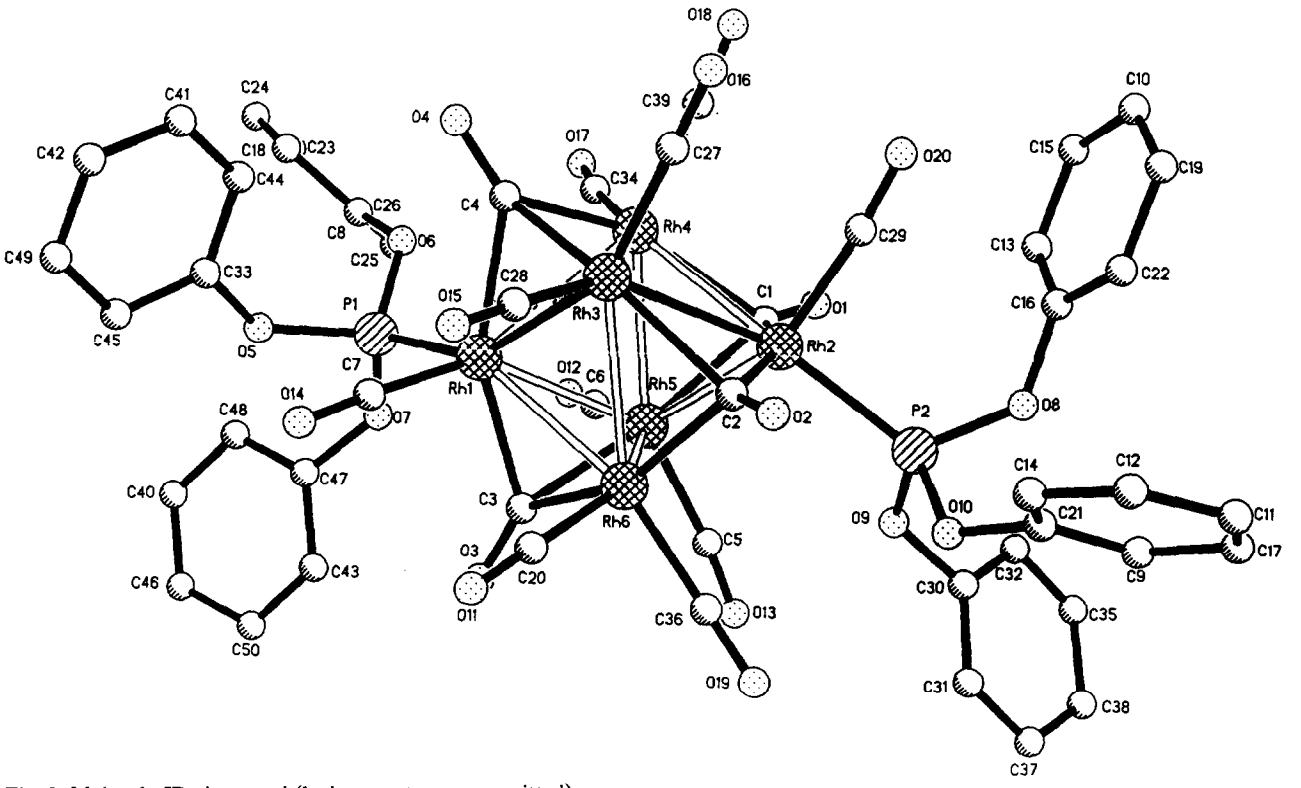

Fig. 3. Molecule IBa in crystal (hydrogen atoms are omitted).

The isomers **2** and **3** have been chosen for the spectrum simulation as compounds with the minimal sterical hindrances between the adjacent phosphite ligands. It should also be noted that the isomer **5** would be expected to have a very simple ^{31}P NMR spectrum due to the high symmetry of its molecule, but neither of the two patterns separated in the experimental spectrum corresponds to the assumed spectrum of **5**. The application of the line narrowing procedure to the experimental spectrum revealed the fine structure of the signals (Fig. 7d). The spectral features clearly show that they are defined not only by the first order [^1J(Rh–P)] couplings but also by the higher ones —^2J(Rh–P) and ^3J(P $\cdots$ P). The diagrams of the spin couplings in the isomers **2** and **3** used in the spectrum simulation are shown in Fig. 8. It should be pointed out that the second order Rh–Rh–P couplings were taken into account only for *trans* (relative to P) Rh atoms as it was done in the interpretation of the ^{31}P NMR spectrum of (I). The spin coupling selection for the isomers **2** and **3** was based upon the structural data for (I) assuming the similarity of the general features of (I) to those of **2** and **3**. The results of PANIC simulation [10] of the ^{31}P spectra for **2** and **3** and the comparison of their superposition with the experimental pattern are given in Fig. 7. It is clear that the superposition of the simulated spectra of **2** and **3** is in excellent agreement with the experimental pattern.

Numerical results of the simulation given in Table 3 fit well the specific features of the structures of the isomers. In the structure of **2** the dihedral angle P(1)Rh(6)Rh(2)P(2) is very close to zero, whereas the same angle for **3** is approximately equal to 45°. In accordance with this difference ^3J(P–P) falls to 18.7 Hz for **3** as compared with 182 Hz for **2**. This is in agreement with the general relation between the values of third order coupling constants and the dihedral angles formed by the corresponding bonds [9,11]. Moreover, the calculated first order ^1J(Rh–P) coupling constants for **2** and **3** are typical of the $Rh_6(CO)_{16}$ phosphite derivatives: 241 Hz for (I), 240 Hz for $Rh_6(CO)_{15}P(OPh)_3$ [12] and 250 Hz for $Rh_6(CO)_{12}\{P(OPh)_3\}_4$ [13]. The indirect determination of the second order [^2J(Rh–P)] coupling constants for **2** and **3** gives the values which are very close to the value of 8 Hz determined directly for (I). Attempts to simulate the spectra of **4** and **5** gave pictures that do not reproduce the corresponding parts of the experimental pattern. These results unambiguously show that the compound (II) and (III) formed in reaction (1) correspond to the possible isomers **2** and **3**.

It should be noted that the isomer (I) is more

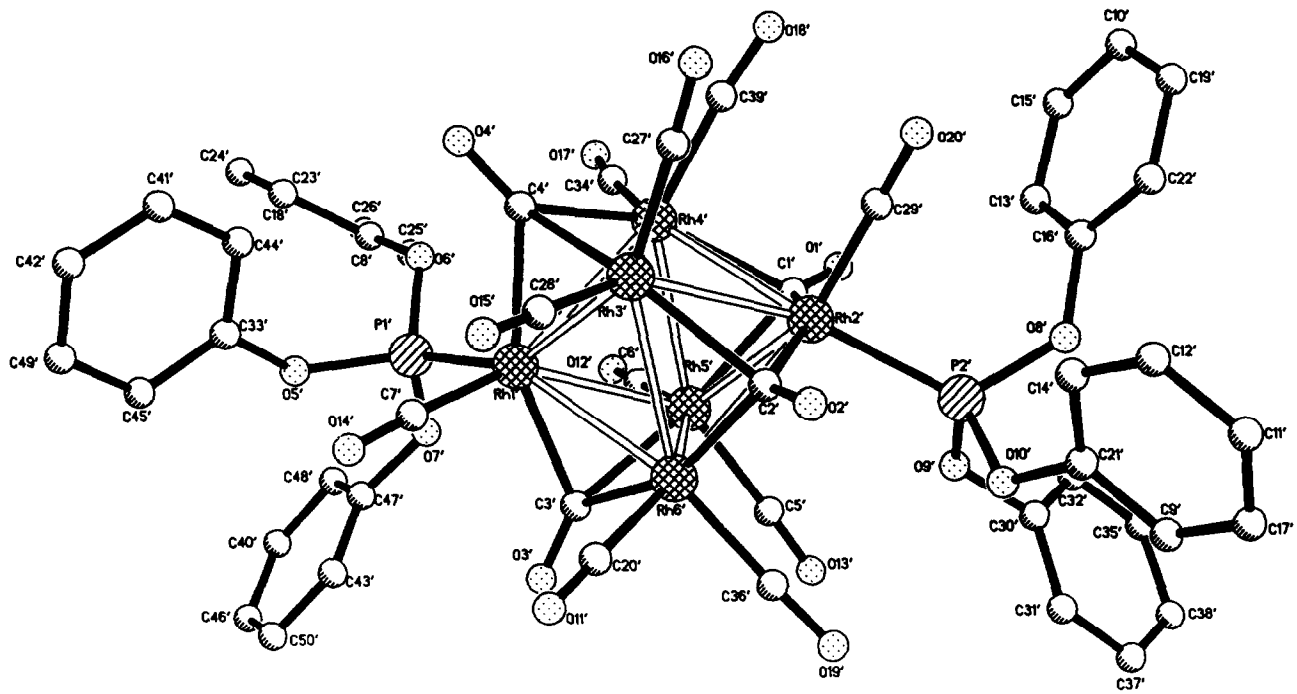

Fig. 4. Molecule IBb in crystal (hydrogen atoms are omitted).)

thermodynamically stable than (II) and (III). Heating of the (I + II + III) mixture results in the irreversible conversion of (II) and (III) into (I) as shown in Fig. 9. However, the distribution of the isomers in the course of reaction (1) is not governed by thermodynamic factors. Analysis of the ^{31}P spectrum of the isomeric mixture obtained after initial separation has shown that relative amounts of the isomers (I), (II) and (III) are approximately 1:2:1 (24.0%, 55%, and 21%). An explanation can be based on the stepwise character of the reaction and the nature of the reaction intermediates. A monosubstituted species formed in the first stage of the reaction is then attacked by Me_3NO with the formation of coordinatively unsaturated intermediate:

$$Rh_6(CO)_{15}P(OPh)_3 + Me_3NO \longrightarrow \{Rh_6(CO)_{14}P(OPh)_3\}^{(*)} + Me_3N + CO_2 \quad (2)$$

The position of the second ligand with respect to the first is controlled by the stereochemistry of the unsaturated intermediate $^{(*)}$, *i.e.*, by the position of the coordination vacancy generated. The almost statistical distribution of the disubstituted products formed suggests either that there is no priority for the attack of Me_3NO on terminal CO or the intermediate $^{(*)}$ is highly stereochemically nonrigid. Both these factors lead to the obtained distribution of the isomers but the latter seems to be more important because, for example, substitution of two NCMe ligands by $P(OPh)_3$ in $Rh_6(CO)_{14}(NCMe)_2$, which easily generates a coordination vacancy via NCMe dissociation, results in the same product distribution. The mechanism of the nonrigidity of the CO environment in the coordinatively unsaturated intermediate $^{(*)}$ apparently includes the coordination vacancy migration via μ_3-CO ↔ t-CO ↔ μ_3-CO rearrangement that is very natural for the coordination vacancy and adjacent bridging CO. Thus, the vacancy is statistically distributed in $^{(*)}$ between eleven terminal sites three of which, corresponding to the isomers **4** and **5**, are sterically inaccessible and the remaining eight sites give rise to the isomers **1–3** with statistical weightings 1:2:1. The conversion of the isomers **2** and **3** into **1** is thought to be governed by a similar dissociation of CO ligands on heating and a consequent t-μ-t migration of phosphite ligands.

2.3. $L = Py$

The disubstituted pyridine derivative of $Rh_6(CO)_{16}$ was synthesized according to reaction (1). Preliminary chromatographic separation yielded a wide band containing a mixture of products with $Rh_6(CO)_{14}(Py)_2$ stoichiometry. We failed to isolate the individual compounds from the mixture due to their ability to interconvert at ambient temperature. An arbitrary separation of this wide band into two parts gave mixtures with different PMR spectral characteristics (Fig. 10(b),

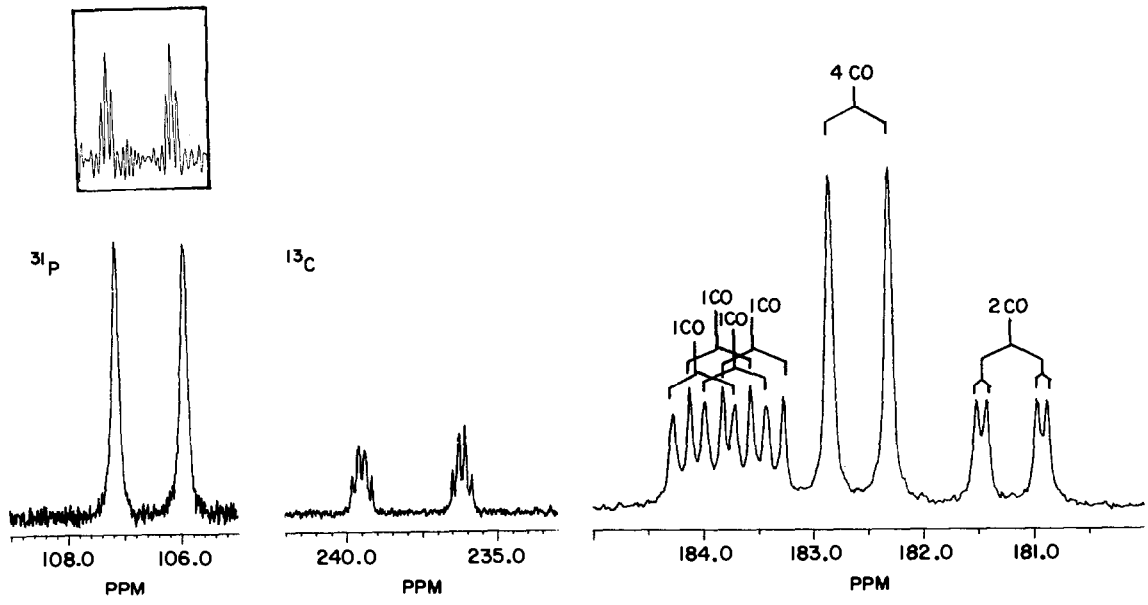

Fig. 5. The ^{13}C and ^{31}P NMR spectra of the compound I ($CDCl_3$, 25°C, ppm, relative to 85% H_3PO_4 for δ ^{31}P). The inset ^{31}P spectrum was obtained using line-narrowing procedure (LB = 21.0, GB = 0.75), $^1J(Rh-P) = 241$ Hz, $^2J(Rh-P) = 8$ Hz. The values of coupling constants in the ^{13}C spectrum: mean $^1J(Rh-C) = 25$ Hz for μ_3-CO, mean $^1J(Rh-C) = 69$ Hz for t-CO, $^2J(P-C) = 11$ Hz.

TABLE 1. Selected Bond Lengths (A) in Compounds IA and IB

Bond	IA	IBa	IBb
Rh1–Rh3	2.756(2)	2.750(1)	2.756(1)
Rh1–Rh4	2.785(2)	2.796(1)	2.786(1)
Rh1–Rh5	2.810(2)	2.788(1)	2.789(1)
Rh1–Rh6	2.778(2)	2.808(1)	2.789(1)
Rh2–Rh3	2.769(2)	2.765(1)	2.768(1)
Rh2–Rh4	2.780(2)	2.767(1)	2.759(1)
Rh2–Rh5	2.790(2)	2.809(1)	2.841(1)
Rh2–Rh6	2.802(2)	2.781(1)	2.783(1)
Rh3–Rh4	2.752(2)	2.761(1)	2.762(1)
Rh3–Rh6	2.756(2)	2.754(1)	2.771(1)
Rh4–Rh5	2.741(2)	2.734(1)	2.740(1)
Rh5–Rh6	2.735(2)	2.732(1)	2.719(1)
Rh1–P1	2.254(5)	2.263(2)	2.261(2)
Rh2–P2	2.243(5)	2.253(2)	2.248(2)
Rh1–C3	2.105(22)	2.141(7)	2.130(7)
Rh1–C4	2.151(21)	2.190(8)	2.194(8)
Rh2–C1	2.154(16)	2.124(7)	2.150(8)
Rh2–C2	2.162(18)	2.154(7)	2.166(7)
Rh3–C2	2.244(21)	2.211(8)	2.220(7)
Rh3–C4	2.227(17)	2.222(8)	2.228(8)
Rh4–C1	2.288(18)	2.300(8)	2.316(7)
Rh4–C4	2.182(15)	2.153(9)	2.140(7)
Rh5–C1	2.201(18)	2.183(8)	2.151(7)
Rh5–C3	2.225(19)	2.197(8)	2.177(7)
Rh6–C2	2.156(21)	2.187(7)	2.134(8)
Rh6–C3	2.228(19)	2.221(7)	2.236(8)
P1–O5	1.57(1)	1.603(6)	1.607(5)
P1–O6	1.59(1)	1.605(5)	1.601(5)
P1–O7	1.61(1)	1.593(5)	1.602(5)
P2–O8	1.59(1)	1.594(6)	1.591(5)
P2–O9	1.60(1)	1.585(5)	1.588(5)
P2–O1	1.59(1)	1.609(5)	1.608(5)
Selected Average Bond Lengths			
$Rh–C(O)_{term}$	2.880	1.904	1.904
$Rh–C(O)_{\mu^3}$	2.194	2.172	2.187
$C–O_{term}$	1.13	1.14	1.13
$C–O_{\mu^3}$	1.17	1.17	1.18
Rh–P	2.248	2.258	2.255

TABLE 2. Selected Bond Angles (deg) in the Compounds IA, IB

Angle	IA	IBa	IBb
RH1–C7–O14	174.3(16)	177.0(7)	177.1(7)
RH2–C29–O20	174.7(17)	173.6(8)	174.9(6)
RH3–C27–O16	175.6(19)	178.3(8)	177.7(6)
RH3–C28–O15	176.7(19)	178.0(7)	178.6(8)
RH4–C34–O17	176.6(18)	173.5(8)	175.5(7)
RH4–C39–O18	178.3(16)	177.7(9)	173.6(7)
RH5–C5–O13	178.1(17)	173.6(7)	176.7(7)
RH5–C6–O12	177.4(19)	178.0(7)	177.8(6)
RH6–C20–O11	171.0(21)	178.9(7)	178.0(8)
RH6–C36–O19	169.9(16)	178.8(6)	177.9(7)
RH2–C1–O1	134.8(13)	137.0(6)	138.6(6)
RH4–C1–O1	132.6(14)	130.4(6)	128.5(5)
RH5–C1–O1	132.1(14)	132.1(6)	131.3(6)
RH2–C2–O2	136.7(14)	137.6(7)	134.6(6)
RH3–C2–O2	130.5(16)	129.9(6)	130.0(5)
RH6–C2–O2	131.1(17)	131.0(6)	132.8(5)
RH1–C3–O3	136.8(16)	135.2(6)	134.5(5)
RH5–C3–O3	131.7(15)	133.2(6)	132.2(5)
RH6–C3–O3	129.4(15)	129.9(5)	131.9(5)
RH1–C4–O4	136.9(13)	137.6(6)	135.1(6)
RH3–C4–O4	130.1(14)	128.5(5)	130.6(6)
RH4–C4–O4	132.0(14)	132.5(6)	133.3(5)
RH3–RH1–P1	152.0(2)	150.0(1)	151.5(1)
RH4–RH1–P1	103.7(1)	102.2(1)	103.5(1)
RH5–RH1–P1	102.0(1)	102.2(1)	101.4(1)
RH6–RH1–P1	147.2(2)	149.1(1)	147.3(1)
RH3–RH2–P2	150.4(1)	150.9(1)	150.3(1)
RH4–RH2–P2	149.3(1)	147.7(1)	149.1(1)
RH5–RH2–P2	103.4(1)	101.7(1)	104.4(1)
RH6–RH2–P2	103.8(2)	102.2(1)	103.9(1)

10(c)), and consequently with a different isomeric composition, but re-equilibration of the separated fractions in solution occurred on standing. A comparison of the spectrum given in Fig. 10(a) with that of the monosubstituted $Rh_6(CO)_{15}Py$ cluster [2] (δ, ppm, 7.45 (t, $2H_\beta$), 7.84 (t, H_γ), 8.98 (d, $2H_\alpha$)) clearly shows that the well resolved lowfield set of doublets corresponds to the H_α protons of coordinated Py in $Rh_6(CO)_{14}(Py)_2$. This pattern can be assigned in the following way. The doublets α_1 and α_3 are likely to be the signals of two individual isomers with equivalent pyridine ligands, whereas two doublets of equal intensity (α_2, α'_2) are presumably the signals of inequivalent Py ligands in isomer **3**. A similar picture is observed in the ^{13}C NMR spectrum of the isomeric mixture. In the region of pyridine carbons (125–155 ppm), Fig. 11, three groups of signals appear, each containing four resonances that

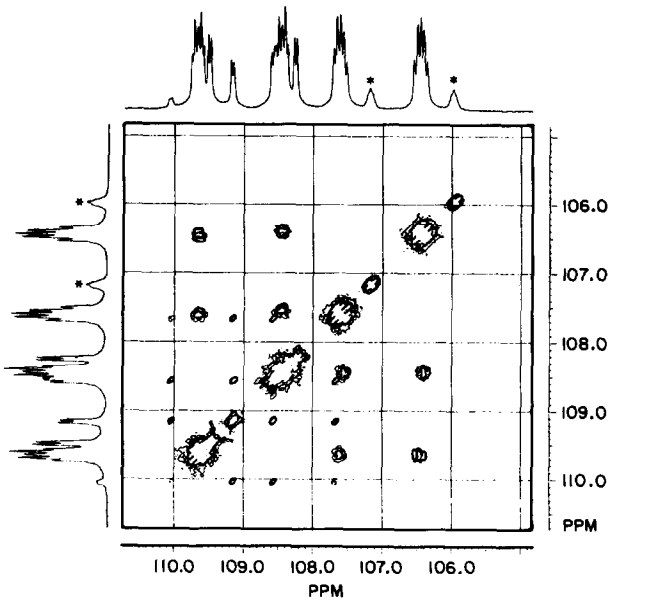

Fig. 6. The 202.458 MHz COSY 90 ^{31}P spectrum of the mixture of (II) and (III) ($CDCl_3$, δ relative to 85% H_3PO_4, 25°C). The asterisk denotes the signals due to the admixture of (I).

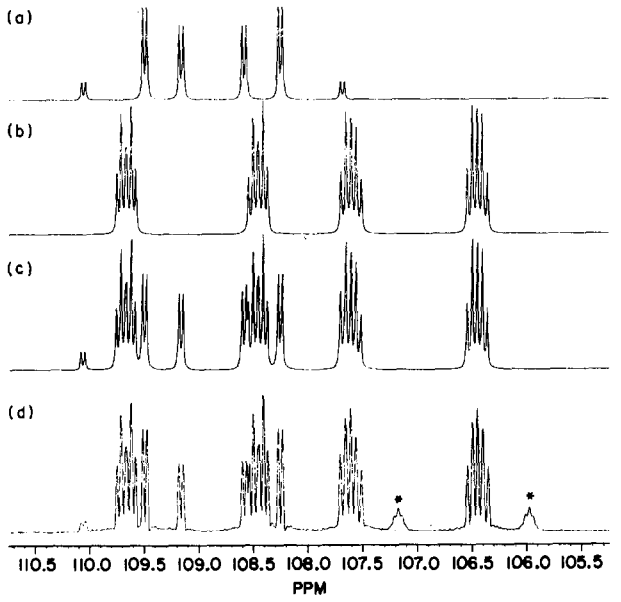

Fig. 7. PANIC simulation of the ^{31}P spectra of the isomers **2** (a) and **3** (b). (c) Superposition of the (a) and (b) spectra. (d) Experimental spectrum of the mixture of (II) and (III) treated with the line-narrowing procedure (LB = −5.0, GB = 0.5). The asterisk denotes the signals due to the admixture of (I).

can be assigned in a manner similar to that of ^1H spectrum. The process of the reequilibration mentioned above is most likely to be connected with the formation of a coordination vacancy via Py ligand dissociation, and the vacancy migration into another terminal position. This process makes the complete separation of the isomers impossible but its rate is not very high and some enrichment of the fractions with the different isomers can be obtained in chromatographic separation.

2.4. L = NCMe

The behaviour of the disubstituted $Rh_6(CO)_{14}(NCMe)_2$ derivative differs significantly from that of the $Rh_6(CO)_{14}(Py)_2$ and $Rh_6(CO)_{14}\{P(OPh)_3\}_2$ clusters. The main product obtained in reaction (1) with the $Rh_6(CO)_{14}(NCMe)_2$ stoichiometry shows no tendency

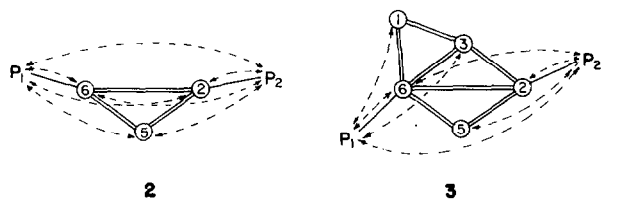

2 3

Fig. 8. Schematic representation of the spin couplings for the isomers **2** (five spin A_2X_2Y system) and **3** (seven spin system). ——— P-Rh and ═══ Rh-Rh bonds, - - - - - - directions of the spin couplings taken into account.

TABLE 3. Results of PANIC simulation of the ^{31}P spectra for the isomers **2** (five spin system) and **3** (seven spin system) (J in Hz)

Isomer **2**	Isomer **3**
$^1J(Rh_2-P_2) = {}^1J(Rh_6-P_1) = 244.0$	$^1J(Rh_2-P_2) = 245.0$; $^1J(Rh_6-P_1) = 244.0$
$^2J(Rh_6-P_2) = {}^2J(Rh_2-P_1) = 7.4$	$^2J(Rh_6-P_2) = {}^2J(Rh_5-P_2) = 8.3$
$^2J(Rh_5-P_1) = {}^2J(Rh_5-P_2) = 7.4$	$^2J(Rh_1-P_1) = {}^2J(Rh_3-P_1) = 9.4$
$^3J(P_2-P_1) = 182.0$	$^3J(P_2-P_1) = 18.7$

to chromatographic separation into the fractions containing the individual isomers in spite of the clear spectroscopic evidence for the presence of a few compounds in the separated band. The ^{13}C NMR spectrum in the carbonyl region (Fig. 12) reveals a very complex pattern corresponding to the mixture of at least two compounds. Moreover, decreasing the temperature to 210 K changes the relative intensities of the signals, pointing to a shift in the equilibrium between the components of the mixture. However, on the basis of the data obtained it is hard to estimate the number of the $Rh_6(CO)_{14}(NCMe)_2$ isomers that prevail in solution. The rate of equilibration is sufficient to display the shift even at very low temperatures. This fact, along with the impossibility of chromatographic separation, suggests that the rate of interconversion of the compounds (isomers) is lower than the characteristic

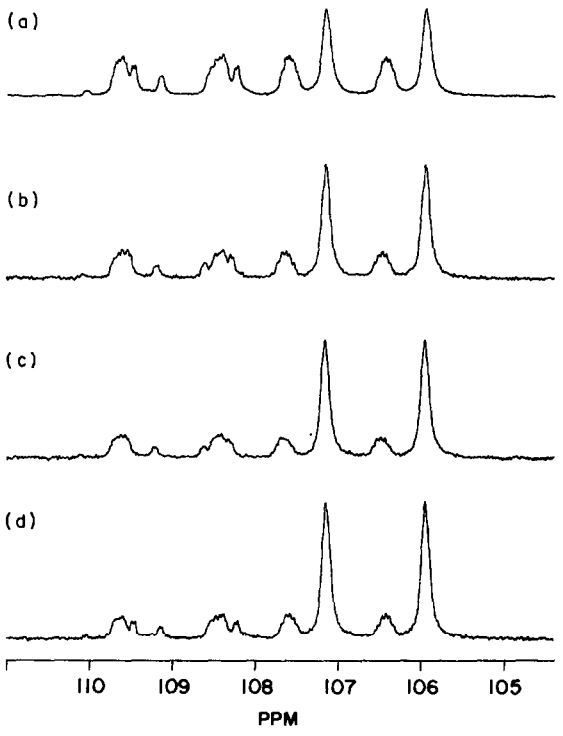

Fig. 9. Variable-temperature ^{31}P NMR spectrum of the mixture of the (I), (II) and (III) compounds, $CDCl_3$. (a) 297 K; (b) 313 K; (c) 323 K; (d) the sample (c) cooled to 303 K.

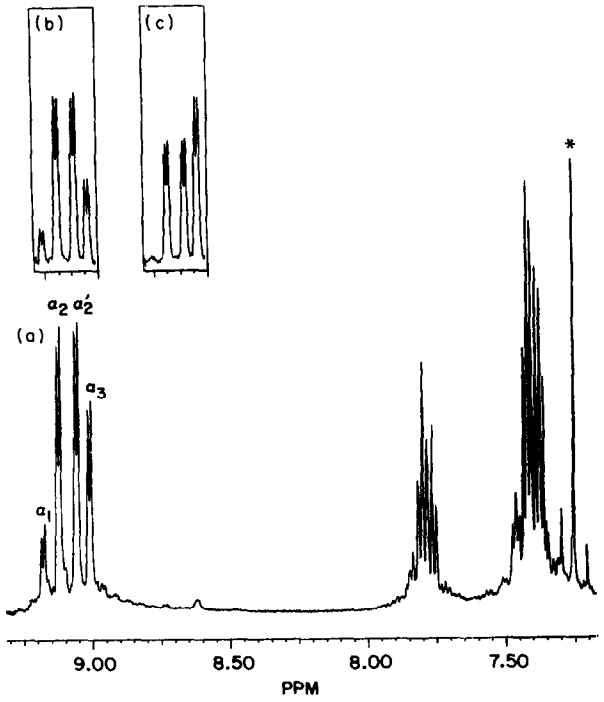

Fig. 10. The ^1H NMR spectra of the mixture of $Rh_6(CO)_{14}(Py)_2$ isomers, $CDCl_3$, 298 K, asterisk denotes the signal of the solvent protons. (a) The mixture after initial separation; (b) and (c) the signals of the H_α pyridine protons in the bands obtained after chromatographic separation of the (a) mixture into two parts.

NMR time scale but much higher than the "separation time scale", *e.g.*, TLC spot test. A suitable mechanism of interconversion is presumably the same as that proposed above including the principal stage of NCMe dissociation and formation of coordination vacancy. This is consistent with the well known lability of the acetonitrile ligand in carbonyl clusters and with the results of independent spectroscopic study of NCMe dissociation from the $Rh_6(CO)_{15}NCMe$ cluster [16].

Thus, the synthesis of the disubstituted derivatives $Rh_6(CO)_{14}L_2$ using Me_3NO yields in the case of $L = P(OPh)_3$ a mixture of three isomers of the possible five, the content of the isomers obtained being governed by pure statistical factors. The other two isomers are sterically crowded and are not formed in the reaction. In the case of L = NCMe and Py the disubstituted compounds obtained are labile and are able to interconvert each other.

3. Experimental section

3.1. Reagent and solvents

Reagent grade $P(OPh)_3$, pyridine, and $Me_3NO \cdot 2H_2O$ were used without further purification. $Rh_6(CO)_{16}$ was obtained by refluxing for 5 h a hexane solution of $Rh_4(CO)_{12}$ which was synthesized according

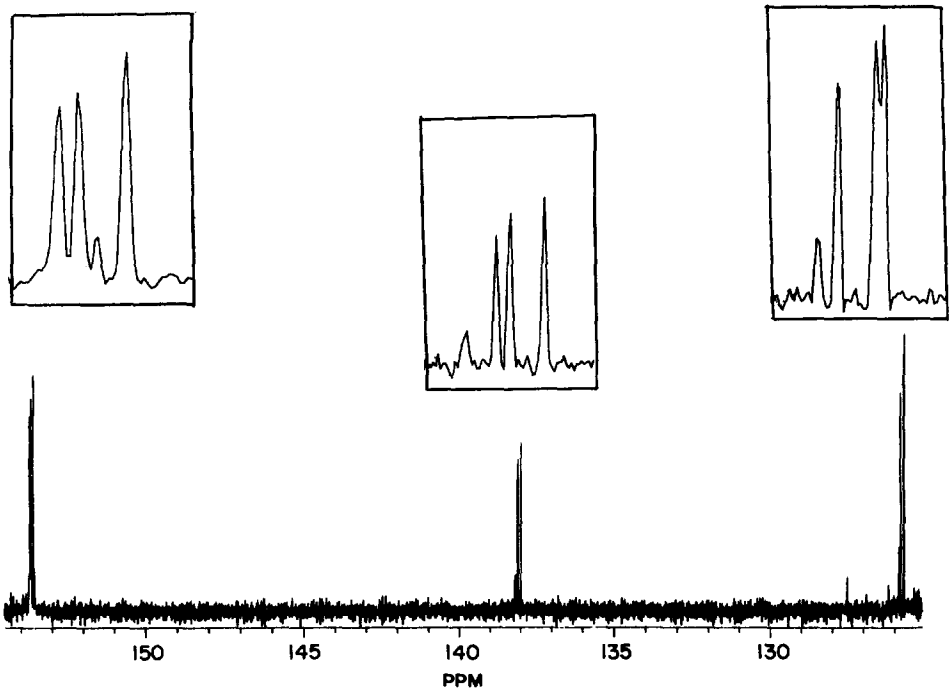

Fig. 11. The ^{13}C NMR spectrum of the mixture of $Rh_6(CO)_{14}(Py)_2$ isomers in the pyridine carbons region, $CDCl_3$, 298 K.

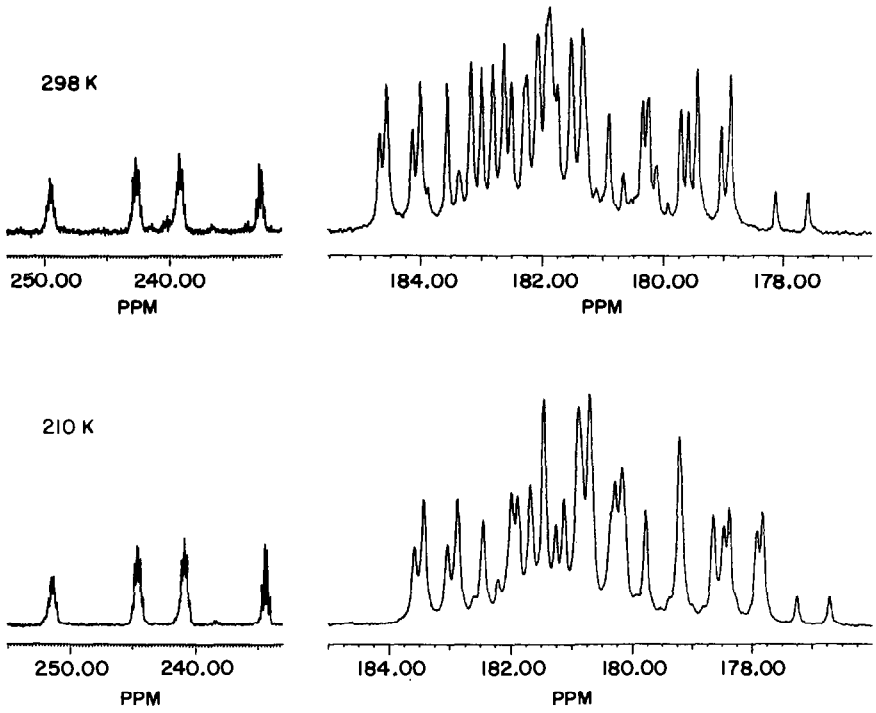

Fig. 12. Variable-temperature ^{13}C NMR spectrum of $Rh_6(CO)_{14}(NCMe)_2$ in the carbonyl region, $CDCl_3$.

to the published procedure [15]. Corresponding ^{13}CO labelled products were obtained from $Rh_4(CO)_{12}$ (20% enriched). All solvents were dried over appropriate reagents and distilled prior to use. Products were separated in air by column chromatography on silica (Silpearl). The ^1H, ^{13}C and ^{31}P NMR spectra were recorded on a Bruker AM-500 instrument. The ^{13}C spectra were recorded using ^{13}CO enriched samples and $Cr(acac)_3$ as a relaxation agent. The ^{31}P NMR study of the phosphite derivatives was performed using the samples with the natural abundance of ^{13}CO to avoid $^{13}C-^{31}P$ coupling. The IR spectra were measured on a Specord M80 spectrophotometer.

3.2. Synthesis of $Rh_6(CO)_{14}\{P(OPh)_3\}_2$

$Rh_6(CO)_{16}$ (50 mg, 0.047 mmol) and 0.03 ml (0.12 mmol) of $P(OPh)_3$ were dissolved in 60 ml of chloroform. A solution of $Me_3NO \cdot 2H_2O$ (11 mg, 0.1 mmol) in $CHCl_3$/MeOH (10/0.5 ml) mixture was added dropwise under vigorous stirring to the cluster solution. The mixture was allowed to stand for an additional 15 min. The solution was then reduced in volume to about 5 ml under vacuum, diluted with hexane (10 ml) and transferred to chromatographic column (3 × 6 cm, Silica 40-100 mesh). Elution with hexane/ether (2/1) gave the following bands in the order of elution: 1) trace of $Rh_6(CO)_{15}P(OPh)_3$ 2) the main dark brown band containing $Rh_6(CO)_{14}\{P(OPh)_3\}_2$, 3) trace of polysubstituted derivatives. Heptane was added to the second fraction, and the solvents were removed under reduced pressure until precipitation of the product. The precipitate was washed with pentane and dried in an air flow. A mixture of the $Rh_6(CO)_{14}\{P(OPh)_3\}_2$ isomers was obtained as a dark brown crystalline powder. Yield 46 mg, 60%.

This mixture was subjected to careful separation on a chromatographic column (10 × 3 cm) with hexane/ether (4/1) as the eluant. Two closely eluted brown bands were separated: the first contained the individual compound (I) and the wide second band proved to be the mixture of two compounds (II and III) of the $Rh_6(CO)_{14}\{P(OPh)_3\}_2$ composition. The IR spectra (ν CO, cm^{-1}, $CHCl_3$); (I) 2094w, 2061s, 2037m, 1783m,br; (II + III) 2094w, 2062s, 2038m, 1783m,br. The composition of (II + III) mixture: found,: C 37.01, H 2.11; calculated for $C_{50}H_{30}O_{20}P_2Rh_6$, C 36.84, H 1.86%.

3.3. Synthesis of $Rh_6(CO)_{14}(Py)_2$

$Rh_6(CO)_{16}$ (50 mg, 0.047 mmol) and 0.01 ml (0.12 mmol) of pyridine were dissolved in 75 ml of chloroform. A solution of $Me_3NO \cdot 2H_2O$ (11 mg, 0.1 mmol) in $CHCl_3$/MeOH (10/0.5 ml) mixture was added dropwise under vigorous stirring to the cluster solution. The mixture was allowed to stand for an additional 15

min. The solution was then reduced in volume to about 5 ml under vacuum, diluted with hexane (10 ml) and separated on a chromatographic column (3 × 6 cm, Silica 40-100 mesh). Elution with hexane/ether (2/1) gave the following bands in the order of elution: 1) trace of $Rh_6(CO)_{15}Py$, 2) the wide dark brown band containing $Rh_6(CO)_{14}(Py)_2$ 3), trace of polysubstituted derivatives. The solvents were removed from the second fraction under reduced pressure. The mixture of the $Rh_6(CO)_{14}(Py)_2$ isomers was obtained as a light brown powder. Yield 34 mg, 62%. Found, C 25.80, H 1.43, N 1.99. Calculated for $C_{24}H_{10}N_2O_{14}Rh_6$, C 24.68, H 0.86, N 2.40%. The IR spectra (ν CO, cm^{-1}, $CHCl_3$); 2090w, 2056s, 2028m, 1776m,br.

3.4. Synthesis of $Rh_6(CO)_{14}(NCMe)_2$

$Rh_6(CO)_{16}$ (100 mg, 0.094 mmol) was dissolved in the mixture of chloroform (120 ml) and acetonitrile (10 ml). The solution of trimethylamine N-oxide ($Me_3NO \cdot 2H_2O$) (22 mg, 0.2 mmol) in 10 ml of MeOH was added dropwise under vigorous stirring to the cluster solution. The mixture was allowed to stand for an additional 15 min. The solution was then reduced in volume to about 30 ml under vacuum, diluted with heptane (20 ml) and concentrated again to 30 ml. This mixture was transferred to chromatographic column (3 × 8 cm, Silicagel 40-100 mesh) and eluted with hexane/chloroform/acetonitrile (15/15/1) mixture. The following bands were separated in the order of elution:

TABLE 4. Atom coordinates in IA (×10^4)

	x	y	z		x	y	z
Rh(1)	8296(2)	7512(1)	593(1)	C(12)	4742(27)	10461(15)	−2352(11)
Rh(2)	7029(2)	8362(1)	−722(1)	C(13)	7670(24)	7232(11)	−2353(8)
Rh(3)	6710(2)	8609(1)	261(1)	C(14)	5428(24)	9833(11)	−2320(8)
Rh(4)	6138(2)	7329(1)	−140(1)	C(15)	7502(28)	7027(13)	−2843(11)
Rh(5)	8651(2)	7251(1)	−400(1)	C(16)	8063(19)	7891(10)	−2248(6)
Rh(6)	9238(2)	8519(1)	4(1)	C(17)	5578(26)	10735(11)	−1525(10)
P(1)	8605(6)	6463(2)	941(2)	C(18)	6805(21)	5056(9)	1345(7)
P(2)	7780(6)	8686(2)	−1428(2)	C(19)	8054(26)	8146(14)	−3105(8)
O(1)	6367(14)	6979(6)	−1255(4)	C(20)	9999(23)	9040(10)	555(7)
O(2)	7748(14)	9837(6)	−327(4)	C(21)	6161(21)	9677(10)	−1866(7)
O(3)	11183(14)	7347(7)	391(5)	C(22)	8207(24)	8335(11)	−2622(7)
O(4)	5495(14)	7550(7)	927(5)	C(23)	7147(24)	3874(10)	1121(8)
O(5)	9766(13)	6040(6)	757(4)	C(24)	6706(22)	4361(12)	1427(8)
O(6)	7354(13)	5975(5)	807(5)	C(25)	7750(22)	4788(9)	591(7)
O(7)	8986(13)	6371(5)	1533(4)	C(26)	7338(20)	5264(8)	913(6)
O(8)	8277(13)	8073(6)	−1746(4)	C(27)	5042(20)	8992(11)	125(8)
O(9)	9018(12)	9196(6)	−1330(4)	C(28)	7134(23)	9219(11)	805(7)
O(10)	6800(13)	9040(6)	−1861(4)	C(29)	5333(19)	8641(9)	−1000(6)
O(11)	10606(20)	9314(9)	875(6)	C(30)	9797(23)	9434(10)	−1694(6)
O(12)	9041(16)	5723(6)	−318(5)	C(31)	10891(28)	9038(12)	−1782(8)
O(13)	10555(15)	7359(7)	−1154(5)	C(32)	9475(26)	10036(11)	−1933(7)
O(14)	9290(17)	8255(7)	1535(4)	C(33)	10900(25)	5674(10)	988(7)
O(15)	7386(17)	9601(8)	1108(5)	C(34)	5798(21)	6381(9)	−121(7)
O(16)	3983(17)	9188(10)	32(8)	C(35)	10214(29)	10299(12)	−2280(8)
O(17)	5591(15)	5808(7)	−135(5)	C(36)	10503(20)	8781(10)	−390(7)
O(18)	3195(14)	7604(7)	−404(6)	C(37)	11675(26)	9346(14)	−2107(9)
O(19)	11417(14)	8943(8)	−572(5)	C(38)	11400(31)	9956(14)	−2344(8)
O(20)	4278(14)	8771(8)	−1144(5)	C(39)	4292(18)	7506(9)	−312(6)
C(1)	6760(19)	7288(8)	−898(6)	C(40)	6759(24)	7280(10)	2272(9)
C(2)	7711(23)	9242(9)	−273(7)	C(41)	13153(30)	5378(17)	965(12)
C(3)	10071(21)	7507(10)	271(7)	C(42)	13043(34)	4909(15)	1352(12)
C(4)	6212(21)	7643(9)	635(5)	C(43)	9390(22)	6966(10)	2293(7)
C(5)	9825(20)	7330(10)	−867(7)	C(44)	12063(35)	5758(12)	809(8)
C(6)	8869(20)	6277(8)	−347(6)	C(45)	10736(23)	5202(11)	1348(8)
C(7)	8966(21)	7953(8)	1192(6)	C(46)	7667(32)	7499(11)	2670(9)
C(8)	7649(21)	4109(10)	694(7)	C(47)	8476(26)	6757(9)	1902(7)
C(9)	6266(24)	10123(12)	−1464(8)	C(48)	7168(26)	6906(9)	1881(7)
C(10)	7623(28)	7462(17)	−3212(8)	C(49)	11862(34)	4817(14)	1526(10)
C(11)	4891(29)	10901(13)	−1960(12)	C(50)	8961(23)	7335(9)	2673(6)

TABLE 5. Atom coordinates in IBa and IBb (primed) ($\times 10^4$)

	x	y	z		x	y	z
Rh(1)	10568(1)	4994(1)	7610(1)	Rh(1')	−16327(1)	−10622(1)	−7228(1)
Rh(2)	8135(1)	5242(1)	7566(1)	Rh(2')	−13808(1)	−10363(1)	−7462(1)
Rh(3)	9027(1)	4111(1)	7297(1)	Rh(3')	−15086(1)	−11447(1)	−6926(1)
Rh(4)	9469(1)	5448(1)	6587(1)	Rh(4')	−14900(1)	−10014(1)	−6410(1)
Rh(5)	9700(1)	6151(1)	7901(1)	Rh(5')	−15079(1)	−9508(1)	−7792(1)
Rh(6)	9226(1)	4838(1)	8613(1)	Rh(6')	−15221(1)	−10909(1)	−8319(1)
P(1)	11855(1)	5605(1)	7243(1)	P(1')	−17327(1)	−9966(1)	−6873(1)
P(2)	7222(1)	5757(1)	8244(1)	P(2')	−12769(1)	−9985(1)	−8271(1)
O(1)	8489(3)	6790(3)	6861(3)	O(1')	−13501(3)	−8699(3)	−7000(3)
O(2)	7534(3)	3753(3)	8382(3)	O(2')	−13925(3)	−11941(3)	−8120(3)
O(3)	10957(3)	5778(3)	9088(3)	O(3')	−16680(3)	−10033(3)	−8744(3)
O(4)	10375(3)	4196(3)	6082(3)	O(4')	−16225(3)	−11156(3)	−5615(3)
O(5)	12665(3)	5200(3)	7260(3)	O(5')	−18305(3)	−10362(3)	−6787(3)
O(6)	11836(3)	5919(3)	6431(3)	O(6')	−17095(3)	−9547(3)	−6116(3)
O(7)	12246(3)	6320(3)	7705(3)	O(7')	−17497(3)	−9324(3)	−7412(3)
O(8)	6428(3)	6038(3)	7882(3)	O(8')	−11797(3)	−9762(3)	−8034(3)
O(9)	7689(3)	6497(3)	8621(3)	O(9')	−12968(3)	−9287(3)	−8703(3)
O(10)	6784(3)	5297(3)	8929(3)	O(10')	−12632(3)	−10536(3)	−8922(3)
O(11)	9818(4)	3632(3)	9513(3)	O(11')	−16301(4)	−12285(3)	−8988(3)
O(12)	11045(4)	7390(3)	7337(3)	O(12')	−15804(4)	−8185(3)	−7250(3)
O(13)	9346(4)	7111(3)	9181(3)	O(13')	−14457(3)	−8694(3)	−9191(3)
O(14)	11363(4)	3791(3)	8307(3)	O(14')	−17634(4)	−11973(3)	−7585(3)
O(15)	9494(4)	2721(3)	7951(3)	O(15')	−16146(4)	−12971(3)	−7181(3)
O(16)	7828(4)	3287(3)	6155(3)	O(16')	−14088(4)	−12078(3)	−5746(3)
O(17)	10572(4)	6640(3)	5677(3)	O(17')	−15385(4)	−8695(3)	−5622(3)
O(18)	8447(5)	5016(5)	5217(3)	O(18')	−13503(4)	−10098(3)	−5314(3)
O(19)	8426(4)	5444(3)	9930(3)	O(19')	−14338(3)	−10415(3)	−9741(3)
O(20)	6882(4)	4624(3)	6386(3)	O(20')	−12562(3)	−10912(3)	−6461(3)
C(1)	8715(5)	6269(4)	7106(4)	C(1')	−13937(5)	−9261(4)	−7145(4)
C(2)	8062(5)	4207(4)	8134(4)	C(2')	−14259(5)	−11462(4)	−7891(4)
C(3)	10488(5)	5580(4)	8606(4)	C(3')	−16196(5)	−10173(4)	−8297(4)
C(4)	10112(5)	4512(4)	6561(4)	C(4')	−15888(5)	−10931(4)	−6160(4)
C(5)	9428(5)	6746(4)	8692(4)	C(5')	−14665(5)	−9003(4)	−8676(4)
C(6)	10552(5)	6918(4)	7549(4)	C(6')	−15544(5)	−8691(4)	−7446(4)
C(7)	11071(5)	4250(4)	8024(4)	C(7')	−17151(5)	−11460(4)	−7434(4)
C(8)	13247(6)	7536(5)	5693(4)	C(8')	−17878(6)	−7871(4)	−5550(4)
C(9)	5312(6)	5355(5)	9093(4)	(C9')	−11516(5)	−10962(5)	−9544(4)
C(10)	5345(7)	5664(7)	5834(6)	C(10')	−10645(6)	−9176(5)	−6046(4)
C(11)	4269(6)	4235(5)	9069(5)	C(11')	−10834(6)	−11911(5)	−9033(5)
C(12)	4902(7)	3829(5)	8959(6)	C(12')	−11338(6)	−11923(5)	−8423(4)
C(13)	6391(6)	6349(5)	6619(5)	C(13')	−11682(5)	−9015(4)	−6945(4)
C(14)	5751(6)	4183(5)	8892(5)	C(14')	−11921(5)	−11467(4)	−8368(4)
C(15)	6016(8)	6201(7)	5939(5)	C(15')	−11263(6)	−8825(4)	−6283(4)
C(16)	6078(5)	5888(4)	7182(4)	C(16')	−11433(5)	−9567(4)	−7341(4)
C(17)	4459(6)	4995(5)	9136(5)	C(17')	−10929(6)	−11431(5)	−9596(5)
C(18)	13015(6)	6013(5)	5609(4)	C(18')	−18227(5)	−9384(4)	−5302(4)
C(19)	5009(6)	5210(6)	6407(6)	C(19')	−10387(5)	−9731(5)	−6460(5)
C(20)	9589(5)	4083(4)	9168(4)	C(20')	−15916(5)	−11774(4)	−8739(4)
C(21)	5929(5)	4937(4)	8957(4)	C(21')	−12004(5)	−10982(4)	−8936(4)
C(22)	5379(6)	5331(5)	7102(5)	C(22')	−10795(5)	−9937(4)	−7115(4)
C(23)	13739(6)	7211(5)	5224(4)	C(23')	−18525(5)	−8169(5)	−5085(4)
C(24)	13616(5)	6457(5)	5181(4)	C(24')	−18690(5)	−8924(5)	−4955(4)
C(25)	12624(6)	7106(4)	6114(4)	C(25')	−17396(5)	−8328(4)	−5902(4)
C(26)	12526(5)	6359(4)	6053(4)	C(26')	−17593(5)	−9083(4)	−5783(4)
C(27)	8270(5)	3602(4)	6573(4)	C(27')	−14442(5)	−11833(4)	−6183(4)
C(28)	9314(5)	3236(4)	7695(4)	C(28')	−15758(5)	−12397(4)	−7085(4)
C(29)	7317(5)	4880(4)	6841(4)	C(29')	−13019(5)	−10672(4)	−6829(4)
C(30)	7288(5)	7004(4)	9021(4)	C(30')	−12411(5)	−8864(4)	−9212(4)
C(31)	7230(6)	6923(4)	9762(5)	C(31')	−12399(6)	−9107(4)	−9919(4)
C(32)	7040(5)	7581(4)	8657(5)	C(32')	−11971(6)	−8189(4)	−8989(4)
C(33)	12684(5)	4480(4)	7017(4)	C(33')	−18660(5)	−11031(4)	−6456(4)
C(34)	10212(5)	6196(4)	6027(4)	C(34')	−15239(5)	−9197(4)	−5922(4)

TABLE 5 (*continued*)

	x	y	z		x	y	z
C(35)	6707(6)	8097(5)	9062(6)	C(35')	−11481(6)	−7743(5)	−9492(5)
C(36)	8727(5)	5227(4)	9440(4)	C(36')	−14683(5)	−10599(4)	−9214(4)
C(37)	6890(6)	7434(5)	10152(5)	C(37')	−11922(7)	−8657(5)	−10413(4)
C(38)	6624(6)	8026(5)	9806(6)	C(38')	−11452(6)	−7986(5)	−10206(5)
C(39)	8816(6)	5184(5)	5737(4)	C(39')	−14055(5)	−10082(4)	−5690(4)
C(40)	14527(6)	6863(5)	8161(6)	C(40')	−19356(7)	−8528(6)	−7901(7)
C(41)	12273(8)	3472(6)	6204(7)	C(41')	−18679(6)	−11982(4)	−5574(4)
C(42)	12743(9)	3064(6)	6574(9)	C(42')	−19453(6)	−12333(4)	−5837(4)
C(43)	12954(6)	6572(5)	8832(5)	C(43')	−18599(6)	−9713(5)	−8293(4)
C(44)	12231(6)	4185(5)	6404(5)	C(44')	−18265(5)	−11321(4)	−5881(4)
C(45)	13184(6)	4085(5)	7402(5)	C(45')	−19436(5)	−11379(4)	−6735(4)
C(46)	14474(7)	6955(5)	8892(6)	C(46')	−19697(7)	−8989(7)	−8442(6)
C(47)	13025(5)	6499(4)	8095(4)	C(47')	−18267(5)	−9233(4)	−7751(4)
C(48)	13796(6)	6643(5)	7744(5)	C(48')	−18631(6)	−8649(5)	−7542(5)
C(49)	13199(8)	3347(7)	7168(8)	C(49')	−19832(5)	−12025(5)	−6413(4)
C(50)	13681(7)	6816(5)	9237(5)	C(50')	−19335(5)	−9594(5)	−8644(4)

1) trace of $Rh_6(CO)_{15}NCMe$ 2) the main dark brown band containing $Rh_6(CO)_{14}(NCMe)_2$ 3) trace of polysubstituted derivatives. Heptane was added to the second fraction and the solvents were removed under reduced pressure until precipitation of the product. The precipitate was washed with pentane and dried in air flow. $Rh_6(CO)_{14}(NCMe)_2$ was obtained as dark brown crystalline powder. Yield 68 mg, 69%. Found: C 19.51%, H 1.00%, N 2.26%. Calculated for $C_{18}H_6N_2O_{14}Rh_6$: C 19.91%, H 0.56%, N 2.58%. The IR spectra (ν CO, cm^{-1}, $CHCl_3$); (I) 2092w, 2056s, 2028m, 1776m,br.

3.5. Crystal structure study of (I)

From the ether-hexane solution at 2°C compound (I) crystallizes simultaneously in two distinct forms (IA) and (IB). The X-ray single crystal diffraction experiments for (IA) and (IB) were carried out with an automated four-circle Siemens P3/PC diffractometer at 273 K for (IA) and 144 K for (IB) with the graphite-monochromated Mo Kα radiation. All calculations were performed using SHELXTL PLUS programs [14].

Crystal data for (IA): $C_{50}H_{30}O_{20}P_2Rh_6$, Fw 1630, monoclinic, space group $P2_1/n$, $a = 10.164(4)$, $b = 19.466(4)$, $c = 27.117(5)$ A, $\beta = 97.49(3)°$, $V = 5319.5(6)$ A^3, $Z = 4$, $d_{calc} = 2.07$ g cm^{-3}, μ(Mo Kα) = 19.26 cm^{-1}.

Crystal data for (IB): $C_{50}H_{30}O_{20}P_2Rh_6$, Fw 1630, triclinic, space group $P1$, $a = 15.952(4)$, $b = 18.362(4)$, $c = 18.408(3)$ A, $\alpha = 90.05(2)$, $\beta = 90.19(2)$, $\gamma = 100.31(2)°$, $V = 5304.8(7)$ A^3, $z = 4$, (two crystallographically independent molecules IBa and IBb), $d_{calc} = 2.04$ g cm^{-3}, μ(Mo Kα) = 19.60 cm^{-1}.

Intensities of 7612 (IA) and 12036 (IB) reflections were measured by $\theta/2\theta$ scan technique ($2\theta < 54°$ (IA); $2\theta < 44°$ (IB)); 3469 reflections with $I > 3.05\sigma(I)$ for (IA) and 9046 reflections with $I > 2\sigma(I)$ for (IB) were used in calculations. The structure was solved by direct method. Least squares anisotropic refinement of all non-hydrogen atoms (hydrogen atoms were placed in the calculated positions and refined isotropically) with the weighting scheme $w = 1/[\sigma^2(F_{obs}) + 0.0003\ F_{obs}^2]$ for (IA) and $w = 1/[\sigma^2(F)]$ for (IB) converged at $R = 0.065$, $R_w = 0.52$, GOF = 2.17 and $R = 0.0328$, $R_w = 0.0291$, GOF = 1.73 for (IA) and (IB) respectively. Atomic coordinates are given in Tables 4 and 5.

References

1 B.F.G. Johnson, R.A. Kamarudin, F.J. Lahos, J. Lewis and P.R. Raithby, *J. Chem. Soc., Dalton Trans.* (1988) 1205; A. Bott, J.G. Jeffrey, B.F.G. Johnson and J. Lewis, *J. Organomet. Chem., 394* (1990) 533.

2 S.P. Tunik, A.V. Vlasov, A.B. Nikol'skii, V.V. Kryvikh and M.I. Rybinskaya, *Metallorg. Khim., 3* (1990) 387; in Russian.

3 S.P. Tunik, A.V. Vlasov, A.B. Nikol'skii, V.V. Kryvikh and M.I. Rybinskaya, *Metallorg. Khim., 4* (1991) 586; in Russian.

4 S.P. Tunik, A.V. Vlasov, N.I. Gorshkov, G.L. Starova, A.B. Nikol'skii, M.I. Rybinskaya, A.S. Batsanov and Yu.T. Struchkov, *J. Organomet. Chem., 433* (1992) 189.

5 E.R. Corey, L.F. Dahl and W. Beck, *J. Amer. Chem. Soc., 85* (1963) 1202.

6 G. Ciani, M. Manassero and V.G. Albano, *J. Chem. Soc. Dalton Trans.*, (1981) 515.

7 G. Ciani, J. Garlaschelli, M. Manassero, U. Sartorelli and V.G. Albano, *J. Organomet. Chem., 129* (1977) 25.

8 P.S. Pregosin and R.W. Kunz, *NMR Basic Princ. Progr., 16* (1979) 1.

9 J. Mason (ed.), *Multinuclear NMR*, Plenum, New York, 1987, Ch. 4 and 13.

10 PANIC, Spectral Simulation Program, Bruker Spectrospin, Coventry, 1985.

11 M. Karplus, *J. Chem. Phys., 30* (1959) 11.

12 Unpublished results.

13 W. Abbaud, Y. Ben Taarit, R. Mutin and J.M. Basset, *J. Organomet. Chem., 220* (1981) C15.
14 W. Robinson and G.M. Sheldrick, SHELX, in N.W. Isaacs and M.R. Taylor (eds.), *Crystallographic Computing Techniques and New Technologies*, Oxford University Press, 1988, p. 366.
15 S. Martinengo, P. Chini and G. Giordano, *J. Organomet. Chem., 27* (1971) 389.
16 S.P. Tunik, A.I. Yarmolenko and A.B. Nikol'skii, *Inorg. Chim. Acta, 205* (1993) 71.